RSC Advances

PAPER

View Article Online
View Journal | View Issue

Cite this: *RSC Adv.*, 2017, **7**, 35854

On Au_nAt clusters as potential astatine carriers†

Sławomir Ostrowski, Agnieszka Majkowska-Pilip, Aleksander Bilewicz* and Jan Cz. Dobrowolski*

Received 9th May 2017
Accepted 13th July 2017

DOI: 10.1039/c7ra05224c

rsc.li/rsc-advances

To understand interactions between astatine atoms with gold clusters the Au_nAt and Au_nX clusters, $n = 12$ or 13, X = F, Cl, Br, and I, were calculated at the DFT level using basis sets with a quasi-relativistic pseudopotential and the D3 Grimme correction for the dispersion interactions. Among the studied clusters of various geometries, the interaction energy of At to the clusters is the smallest. Yet, consideration of the electron detachment from the X^- anion and generation of a H_2 molecule and OH^- anion from water shows that the formation of the astatine gold clusters is favored.

Alpha particle emitting isotopes are of considerable interest for radionuclide therapy because of their high cytotoxicity and short path length. Due to the relatively high availability, ^{211}At is actually the most promising α emitter for targeted radiotherapy. Attaching ^{211}At to biomolecules targeting cancer cells is crucial for its application in the radionuclide therapy. Although astatine is generally treated as a halogen (X), it also shows a significant metallic character in certain conditions.[1] The strength of aryl carbon–halogen bond for astatine is significantly lower than that for iodine which precludes the use of standard direct radioiodination methods for labelling monoclonal antibodies (mAbs) with ^{211}At.[2] Such methods lead to unstable products resulting in rapid *in vivo* loss of ^{211}At. It is well known that iodine has a high affinity for the noble metal surface and the degree of specific adsorption of halides on the gold surface increases in the order $F^- < Cl^- < Br^- < I^-$. In particular, the F^- ion has the lowest affinity and, specifically, adsorbs on the metal surface weakly. The Cl^-, Br^-, and I^- ions are able to chemisorb on the gold surface forming an Au–X bond.[3] This phenomenon was applied to elaboration of a new method for iodination of biomolecules using the gold nanoparticle as a metal bridge between ^{125}I and a biomolecule.[4] Taking into account the increasing bond strength between Au surface and the halogen atom in order $F^- < Cl^- < Br^- < I^-$, we can assume that astatide, the heaviest halogen anion, will bind to the Au surface even stronger than iodide. Our recent experimental studies have shown that astatine is indeed very strongly adsorbed on the gold surface and allows to use gold nanoparticles as a bridge between ^{211}At and a biomolecule.[5] Moreover, the ^{211}At bioconjugates were very stable in human blood serum and cerebrospinal fluid.[5]

The aim of this study was to understand interactions between At and gold clusters using computational methods. To ensure a compromise between computational costs and stay close to reality we decided to model At interactions with Au_{13} clusters. The Au_{13} cluster with the central atom surrounded by a single shell of 12 atoms is the first from the class of full-shell clusters.[6] It is known experimentally. Indeed, the crystal structures of $[Au_{13}(PMe_2Ph)_{10}Cl_2](PF_6)_3$ and $[Au_{13}(dppmH)_6](NO_3)_n$, already solved in 1981, contain the centred icosahedral Au cluster.[7,8] Nowadays synthesis of compounds containing Au_{13} cluster is well established.[9]

So indeed, the Au_{13} clusters taken into account here, exist in real world, capture essential chemistry and physics and are more convenient for calculations than Au clusters of a larger size. However, the Au clusters applied in our experimental study on a carrier of the At atoms[5] were synthesized by Turkevich and Brust–Schiffrin method yielding nanoparticle diameters from 20 to 200 Å. Thus, they displayed diameters at least three- to five-fold greater than the clusters considered in this study. Since volume scales as the cube of the radius, the number of the Au atoms in our experimental clusters was at least 350 rather than 13. On the other hand, the aim of this study was to find a rationale for using gold clusters as At carriers not to reproduce an exact cluster parameters. Therefore, the size of the studied clusters is a compromise allowing us estimation of the At interaction (binding) energy to the cluster at the level of theory providing a fairly acceptable accuracy.

The initial icosahedral Au_{13} structure was taken from references[6–9] and optimized at the selected theory level‡ appeared to be slightly distorted (Fig. 1), while if constrained to conserve the

Institute of Chemistry and Nuclear Technology, 16 Dorodna Street, 03-195 Warsaw, Poland. E-mail: a.bilewicz@ichtj.waw.pl; j.dobrowolski@nil.gov.pl; Fax: +48 22 811 1532; +48 22 811 1917; Tel: +48 22 504 1357; +48 22 504 1086

† Electronic supplementary information (ESI) available: Cartesian coordinates of all studied systems and energetics of the selected systems are available. See DOI: 10.1039/c7ra05224c

‡ The computations were performed using the LC-ωPBE functional[10–12] combined with the Stuttgart/Cologne Group (SDD) basis sets with quasi-relativistic pseudopotential[13] and the D3 Grimme correction[14] for the dispersion interactions as implemented in Gaussian 09 suite of programs.[15] For open-shell systems the spin contamination was checked to be small.[16] For more details see ESI.†

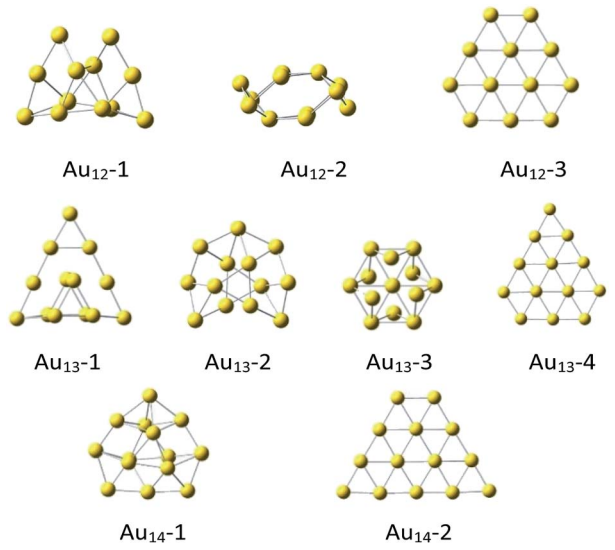

Fig. 1 The DFT optimized‡ Au_{12}, A_{13} and Au_{14} structures.

I_h symmetry, it exhibited imaginary frequencies. Therefore, except the slightly distorted icosahedron (Au_{13}-3, Fig. 1), we took several other high-symmetry geometries considered before for both Au_{12} and Au_{13} clusters (Fig. 1).[17–21]

Notice, that the non-planar Au_{12}-1, Au_{13}-1 and Au_{13}-2, and Au_{14}-1 are the most stable in the cluster of the same size (Table 1). It may seem surprising that the slightly distorted icosahedral Au_{13}-3 structure is less stable than the most stable Au_{13} clusters by 17.5 kcal mol^{-1}. However, in general, the high-symmetry (I_h, O_h, D_{3h}, D_{5h}) Au_{13} clusters tend to be less stable than those of lower symmetry.[17] It is possible that this is a result of lack of external stabilisation forces in vacuum, while in crystals the most packed form of cluster is favorized.[7,13,19] As expected,[18] the planar Au_{12}-3, Au_{13}-4 and Au_{14}-2 clusters are definitely the least stable (Table 1). Energetics of the quartet spin state considered for the Au_{13} systems indicated doublets to be always significantly more stable than quartets (see ESI†).

To model halogen–Au cluster interaction, first, we assumed that the halogen atom interacts with the cluster surface rather than is placed as one of the inner cluster atoms. In the case of planar clusters, introductory calculations indicated that the position in plane is more stable that any of the out of plane ones. Only a few, out of a multitude combinatorially possible, positions of the halogen atom on each Au cluster could be taken into account. For each halogen, the structures of those few positions were optimized. The structures fall into a few types, which however, locally are quite different. This is because in series of halogens, their electronegativities, volumes, ionization potentials, electron affinities, *etc.* differ a lot. The finding for all halogens were generalized, remembering that the objective of this study was to find a tendency for all halogens rather than a strict rule for a given type of cluster.

For all Au_n clusters, series of similar neutral Au_nX structures were optimized (Fig. 2). It appeared that the heavier the halogen the less stable the cluster (Table 2). This is not unexpected because the halogen electronegativity decreases with its mass from 3.98 for fluorine to *ca.* 2.2 for astatine.[22] Indeed, already for the AuX molecules the interaction energies decrease monotonically from *ca.* −110 kcal mol^{-1} for fluorine to −90 kcal mol^{-1} for astatine. For most of the $Au_{12}X$ and $Au_{13}X$ clusters such a trend is preserved, although it is not always monotonic.

Remark, that the $Au_{12}X$-3 structure is the most whereas the $Au_{12}X$-4 one is the least stable. They are derived from the Au_{12}-1 and Au_{12}-3 clusters, respectively, which are the most and the least stable as well. However, the $Au_{12}X$-1 structures are obtained from the most stable Au_{12}-1 cluster, yet, the halogen stabilization energies in this very cluster are similar to the weakest $Au_{12}X$-4 ones.

On the other hand, the most stable $Au_{13}X$-3 structures are obtained from the Au_{13}-2 clusters which are (one of two) the most stable and the least stable $Au_{13}X$-5 structures are obtained from the least stable planar Au_{13}-4 clusters. Notice however, that the $Au_{13}X$-1 and $Au_{13}X$-2 systems were also obtained from the most stable the Au_{13}-1 and Au_{13}-2 clusters but yield $Au_{13}X$ systems which are *ca.* 15 kcal mol^{-1} less stable than $Au_{13}X$-3 ones. Comparison of the geometries of the clusters shows that within the given type of the Au_nX clusters its structure does not vary much with the halogen. In contrast, the site the halogen is attached to the Au_n cluster significantly changes the interaction energy whether the parent gold cluster was very stable or not. Nevertheless, regardless the given Au_nX cluster type the halogen–gold cluster interaction energy decreases from F to At atom. Finally notice, that as for the Au_{13} clusters, the $Au_{12}X$ ones

Table 1 The total energy E (hartree) and energy differences ΔE (kcal mol^{-1}) between different Au_{12}, Au_{13} and Au_{14} clusters (Fig. 1).‡ Energetics for the doublet spin state of the Au_{13} and the singlet spin state of Au_{12} and Au_{14} systems are presented. For Au_{13} quartets see ESI

Cluster	E	ΔE	G_{298}	ΔG_{298} kcal mol^{-1}
Au_{12}-1	−1629.405910	0.0	−1629.474373	0.0
Au_{12}-2	−1629.393431	7.8	−1629.462010	7.8
Au_{12}-3	−1629.357086	30.7	−1629.429677	28.1
Au_{13}-1	−1765.181138	0.0	−1765.254652	0.3
Au_{13}-2	−1765.181041	0.1	−1765.255102	0.0
Au_{13}-3	−1765.153717	17.2	−1765.227080	17.6
Au_{13}-4	−1765.129280	32.6	−1765.206241	30.7
Au_{14}-1	−1901.021432	0.0	−1901.094858	0.0
Au_{14}-2	−1900.902310	74.8	−1900.980926	71.5

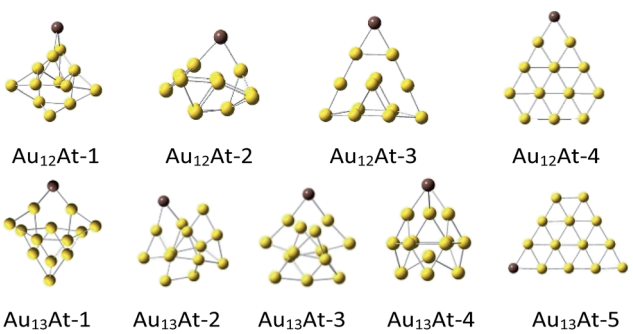

Fig. 2 The DFT optimized‡ $Au_{12}At$ and $Au_{13}At$ structures.

Table 2 The interaction energy (ΔE, kcal mol^{-1}) of the halogen atom X = F, Cl, Br, I, and At with the Au_{12} and Au_{13} clusters.‡ Energetics for the doublet spin state of the $Au_{12}X$ and the singlet spin state of $Au_{1s}X$ are presented. For $Au_{12}X$ quartets see ESI

ΔE	F	Cl	Br	I	At
AuX	−108.77	−101.57	−98.53	−96.23	−92.74
$Au_{12}X$-1	−56.1	−49.4	−45.2	−46.0	−39.0
$Au_{12}X$-2	−57.7	−52.2	−49.8	−52.2	−45.7
$Au_{12}X$-3	−83.8	−75.9	−77.1	−76.3	−68.0
$Au_{12}X$-4	−55.8	−47.7	−43.1	−42.7	−34.8
$Au_{13}X$-1	−96.8	−88.0	−83.8	−83.3	−80.1
$Au_{13}X$-2	−93.7	−86.7	−82.4	−82.3	−79.6
$Au_{13}X$-3	−111.6	−104.6	−100.2	−100.1	−96.1
$Au_{13}X$-4	−86.8	−80.1	−75.7	−75.8	−73.1
$Au_{13}X$-5	−40.4	−31.4	−25.2	−23.0	−19.0

in the quartet spin state are always significantly less stable than doublets (see ESI†).

The decreasing interaction energy between halogen and gold cluster in Au_nX systems as the atomic number of halogen is increased would suggest that the same tendency could obey the gold clusters as a halogen carriers in water environment. In fact, in most cases the opposite is true. For example, in aqueous solutions the degree of specific adsorption on a gold surface increases in the order $F^- < Cl^- < Br^- < I^-$. Especially, F^- has the lowest affinity and only nonspecifically or weakly specifically adsorbs on gold surface. Such an effect was observed in the case of adsorption of halides on gold electrode surfaces[22] and aggregation of gold nanoparticles induced by halides adsorption.[23] Indeed, to form an Au_nX cluster, the X^- halide anion must be oxidized to the X^0 free halogen form. As a result, the released electron is attached to water molecule and the H_2 molecule and OH^- anion are formed:

$$X^- + Au_n + H_2O \rightarrow Au_nX + \tfrac{1}{2}H_2 + OH^- \quad (1)$$

The energy balance of the above reaction demonstrates that the stabilization energy of the halogen atom at the Au_{12} and Au_{13} clusters in water environment tend to increase from F to At (Table 3).

Table 3 The standard reduction potentials for halogens[24,25] X = F, Cl, Br, I, and At (kcal mol^{-1}) and the stabilization energy of the halogen atom at the Au_{12} and Au_{13} clusters in water environment. E^0 for $2H_2O + 2e \rightarrow H_2 + 2OH^-$ is assumed to be equal to −19.08721 kcal mol^{-1}

	X				
System	F	Cl	Br	I	At
$X_2 + 2e \rightarrow 2X^-$	−66.09	−33.90	−26.75	−16.60	−6.00
AuX	−66.18	−75.08	−75.61	−78.38	−80.20
$Au_{12}X$-1	−13.51	−22.91	−22.28	−28.15	−26.46
$Au_{12}X$-2	−15.11	−25.71	−26.88	−34.35	−33.16
$Au_{12}X$-3	−41.21	−49.41	−54.18	−58.45	−55.46
$Au_{12}X$-4	−13.21	−21.21	−20.18	−24.85	−22.26
$Au_{13}X$-1	−54.21	−61.51	−60.88	−65.45	−67.56
$Au_{13}X$-2	−51.11	−60.21	−59.48	−64.45	−67.06
$Au_{13}X$-3	−69.01	−78.11	−77.28	−82.25	−83.56
$Au_{13}X$-4	−44.21	−53.61	−52.78	−57.95	−60.56
$Au_{13}X$-5	2.19	−4.91	−2.28	−5.15	−6.46

In conclusion, we have computationally confirmed the higher stability of the $Au_{12}At$ and $Au_{13}At$ clusters in water environment than stability of the analogous clusters with lighter halogens. Our experimental studies already signalized a high therapeutic potential of ^{211}At labelled gold nanoparticles functionalized with substance P and trastuzumab towards glioma cells and HER2 positive breast and ovarian cancers. These two findings open new perspectives for optimization novel ^{211}At labelled gold nanoparticles functionalized with different biomolecules for cancer targeting therapy.

Acknowledgements

This work was supported by Grant 2013/11/B/ST4/00516 from the National Science Center in Poland. The computational Grant from the Świerk Computing Centre (CIŚ) is gratefully acknowledged. Critical comments of anonymous referees to this paper are gratefully acknowledged.

Notes and references

1 J. Champion, M. Seydou, A. Sabatie-Gogova, E. Renault, G. Montavon and N. Galland, *Phys. Chem. Chem. Phys.*, 2011, **13**, 14984–14992.
2 K. Berei and L. Vasaros, "Organic Chemistry of Astatine", *Hungarian Academy of Sciences*, Central Research Institute for Nuclear Physics, Budapest, 114, Hungary, 1981.
3 Z. Zhang, H. Li, F. Zhang, Y. Wu, Z. Guo, L. Zhou and J. Li, *Langmuir*, 2014, **30**, 2648–2659.
4 Y.-H. Kim, J. Jeon, S. H. Hong, W.-K. Rhim, Y.-S. Lee, H. Youn, J.-K. Chung, M. C. Lee, D. S. Lee, K. W. Kang and J.-M. Nam, *Small*, 2011, **7**, 2052–2060.
5 A. Bilewicz, Ł. Janiszewska, P. Kozmiński, M. Łyczko, M. Pruszyński, J. Jastrzębski, J. Choiński, A. Stolarz, A. Trzcińska, K. Szkliniarz and W. Zipper, *Eur. J. Nucl. Med. Mol. Imaging*, 2015, **42**, S245.
6 G. Schmid, *Metal Nanoparticles: Electronic Properties, Bioresponse, and Synthesis, Encyclopedia of Inorganic and Bioinorganic Chemistry*, Wiley, 2011–2012.
7 C. E. Briant, B. R. C. Theobald, J. W. White, L. K. Bell, D. M. P. Mingos and A. J. Welch, *J. Chem. Soc., Chem. Commun.*, 1981, 201–202.
8 J. W. A. van der Velden, F. A. Vollenbroek, J. J. Bour, P. T. Beurskens, J. M. M. Smits and W. P. Bosnian, *Recl. Trav. Chim. Pays-Bas*, 1981, **100**, 148–152.
9 Y. Shichibu, K. Suzuki and K. Konishi, *Nanoscale*, 2012, **4**, 4125–4129.
10 O. A. Vydrov and G. E. Scuseria, *J. Chem. Phys.*, 2006, **125**, 234109.
11 E. Weintraub, T. M. Henderson and G. E. Scuseria, *J. Chem. Theory Comput.*, 2009, **5**, 754–762.
12 B. Civalleri, D. Presti, R. Dovesia and A. Savin, *Chem. Modell.*, 2012, **9**, 168–185.
13 http://www.tc.uni-koeln.de/PP/clickpse.en.html.

14 S. Grimme, J. Antony, S. Ehrlich and H. Krieg, *J. Chem. Phys.*, 2010, **132**, 154104.
15 M. J. Frisch, G. W. Trucks, H. B. Schlegel, G. E. Scuseria, M. A. Robb, J. R. Cheeseman, G. Scalmani, V. Barone, B. Mennucci, G. A. Petersson, H. Nakatsuji, M. Caricato, X. Li, H. P. Hratchian, A. F. Izmaylov, J. Bloino, G. Zheng, J. L. Sonnenberg, M. Hada, M. Ehara, K. Toyota, R. Fukuda, J. Hasegawa, M. Ishida, T. Nakajima, Y. Honda, O. Kitao, H. Nakai, T. Vreven, J. A. Montgomery, J. E. Peralta, F. Ogliaro, M. Bearpark, J. J. Heyd, E. Brothers, K. N. Kudin, V. N. Staroverov, R. Kobayashi, J. Normand, K. Raghavachari, A. Rendell, J. C. Burant, S. S. Iyengar, J. Tomasi, M. Cossi, N. Rega, N. J. Millam, M. Klene, J. E. Knox, J. B. Cross, V. Bakken, C. Adamo, J. Jaramillo, R. Gomperts, R. E. Stratmann, O. Yazyev, A. J. Austin, R. Cammi, C. Pomelli, J. W. Ochterski, R. L. Martin, K. Morokuma, V. G. Zakrzewski, G. A. Voth, P. Salvador, J. J. Dannenberg, S. Dapprich, A. D. Daniels, O. Farkas, J. B. Foresman, J. V. Ortiz, J. Cioslowski and D. J. Fox, *Gaussian 09, Revision C.01*, Gaussian, Inc., Wallingford CT, 2009.
16 A. S. Menon and L. Radom, *J. Phys. Chem. A*, 2008, **112**, 13225–13230.
17 J. Sun, X. Xie, B. Cao and H. Duan, *Comput. Theor. Chem.*, 2017, **1107**, 127–135.
18 D. A. Götz, R. Schäfer and P. Schwerdtfeger, *J. Comput. Chem.*, 2013, **34**, 1975–1981.
19 S. Takano, S. Yamazoe and T. Tsukuda, *APL Mater.*, 2017, **5**, 053402.
20 H. M. Lee, M. Ge, B. R. Sahu, P. Tarakeshwar and K. S. Kim, *J. Phys. Chem. B*, 2003, **107**, 9994–10005.
21 H. Häkkinen, B. Yoon, U. Landman, X. Li, H.-J. Zhai and L.-S. Wang, *J. Phys. Chem. A*, 2003, **107**, 6168–6175.
22 O. M. Magnussen, *Chem. Rev.*, 2002, **102**, 679–726.
23 Z. Zhang, H. Li, F. Zhang, Y. Wu, Z. Guo, L. Zhou and J. Li, *Langmuir*, 2014, **30**, 2648–2659.
24 *CRC Handbook of Chemistry and Physics*, ed. D. R. Lide, Internet Version 2005, http://www.hbcpnetbase.com, CRC Press, Boca Raton, FL, 2005.
25 J. Champion, C. Alliot, E. Renault, B. M. Mokili, M. Chérel, N. Galland and G. Montavon, *J. Phys. Chem. A*, 2010, **114**, 576–582.